Published May 17, 2010

JEM

Article

One naive T cell, multiple fates in CD8+ T cell differentiation

Carmen Gerlach,[1] Jeroen W.J. van Heijst,[1] Erwin Swart,[1] Daoud Sie,[2] Nicola Armstrong,[3] Ron M. Kerkhoven,[2] Dietmar Zehn,[4] Michael J. Bevan,[5] Koen Schepers,[1] and Ton N.M. Schumacher[1]

[1]Division of Immunology, [2]Central Microarray Facility, and [3]Bioinformatics and Statistics Group, Division of Molecular Biology, The Netherlands Cancer Institute, 1066 CX Amsterdam, Netherlands
[4]Swiss Vaccine Research Institute, 1011 Lausanne, Switzerland
[5]Howard Hughes Medical Institute, University of Washington, Seattle, WA 98195

The mechanism by which the immune system produces effector and memory T cells is largely unclear. To allow a large-scale assessment of the development of single naive T cells into different subsets, we have developed a technology that introduces unique genetic tags (barcodes) into naive T cells. By comparing the barcodes present in antigen-specific effector and memory T cell populations in systemic and local infection models, at different anatomical sites, and for TCR–pMHC interactions of different avidities, we demonstrate that under all conditions tested, individual naive T cells yield both effector and memory CD8+ T cell progeny. This indicates that effector and memory fate decisions are not determined by the nature of the priming antigen-presenting cell or the time of T cell priming. Instead, for both low and high avidity T cells, individual naive T cells have multiple fates and can differentiate into effector and memory T cell subsets.

CORRESPONDENCE
Ton N.M. Schumacher:
t.schumacher@nki.nl

Abbreviations used: 2-D, two dimensional; Ltd, Limited.

Activation of naive antigen-specific T cells is characterized by a vigorous proliferative burst, resulting in the formation of a large pool of effector T cells. After pathogen clearance, ~95% of activated T cells die, leaving behind a stable pool of long-lived memory cells (Williams and Bevan, 2007). Two fundamentally different mechanisms could give rise to the production of effector and memory T cells during an immune response. First, single naive T cells may be destined to produce either effector T cells or memory T cells, but not both ("one naive cell, one fate"). As an alternative, effector and memory T cells could derive from the same clonal precursors within the naive T cell pool ("one naive cell, multiple fates"). As the fate decisions that control T cell differentiation could either be taken during initial T cell priming (i.e., before the first cell division) or at later stages, at least four conceptually different models describing effector and memory T cell differentiation can be formulated (Fig. S1).

A first model predicts a separate origin of effector and memory T cells as a result of differential T cell priming by APCs. In this scenario, fate decisions would be taken before the first cell division, and even though cells destined to become memory cells may transiently display traits associated with effector T cells (e.g., expression of granzyme B or IFN-γ; see the following paragraphs), their ability for long-term survival would be predetermined. In line with this model, several studies have provided evidence that the fate of CD8+ T cells may, to some extent, be programmed during initial activation (Kaech and Ahmed, 2001; van Stipdonk et al., 2003; Masopust et al., 2004; Williams and Bevan, 2007; Bannard et al., 2009).

A second model, which relies on recent data from Chang et al. (2007), likewise suggests that the priming APC plays the crucial role in determining effector or memory T cell fate, but by a strikingly different mechanism and with an opposite prediction concerning the lineage relationship of effector and memory T cells.

N. Armstrong's present address is Sydney Bioinformatics, The University of Sydney, Sydney NSW 2006, Australia.
K. Schepers's present address is the Eli and Edythe Broad Center of Regeneration Medicine and Stem Cell Research, Division of Hematology/Oncology, University of California, San Francisco, San Francisco, CA 94143.

The Rockefeller University Press $30.00
J. Exp. Med. Vol. 207 No. 6 1235-1246
www.jem.org/cgi/doi/10.1084/jem.20091175

Supplemental Material can be found at:
/content/suppl/2010/05/17/jem.20091175.DC1.html

Published May 17, 2010

Specifically, analysis of T cell–APC conjugates has shown that the first division of activated T cells can be asymmetric, with the daughter T cell that is formed proximal to the APC being more likely to contribute to the effector T cell subset and the distal daughter T cell being more likely to generate memory T cells (Chang et al., 2007). Assuming that all primary daughter cells survive and yield further progeny, these data would predict that single naive T cells contribute to both the effector and the memory subset.

In contrast to these two models that are based on a determining role of the priming APC, two other models predict that T cell fate is determined by the cumulative effect of signals that not only naive T cells but also their descendants receive. The first of these models, termed the "decreasing potential model," argues that T cell progeny that receive additional stimulation after priming undergo terminal differentiation toward the effector subset, whereas descendants that do not encounter these signals may transiently display certain effector functions but will ultimately become memory T cells (Ahmed and Gray, 1996). In support of this model, it has been demonstrated that continued inflammatory signals (Badovinac et al., 2004; Joshi et al., 2007) and prolonged antigenic stimulation (Sarkar et al., 2008) can lead descendant $CD8^+$ T cells to preferentially develop into effector cells.

If the descendants of all individual naive T cells have an equal chance of receiving signals for terminal differentiation, the standard decreasing potential model predicts that memory and effector T cells will be derived from the same population of naive T cells. However, there is evidence that the environmental factors that promote either terminal differentiation or memory T cell development may alter over the course of infection (Sarkar et al., 2008). A fourth model therefore argues that the progeny of T cells that are activated early or late during infection will receive distinct signals and, hence, assume (partially) different fates (van Faassen et al., 2005; D'Souza and Hedrick, 2006; Quigley et al., 2007; Stemberger et al., 2007a).

A large number of studies in which cell differentiation was analyzed at the population level have been informative in revealing which effector properties can be displayed by T cells that subsequently differentiate into memory T cells (for review see Jameson and Masopust, 2009). In particular, two recent studies using IFN-γ or granzyme B reporter mice have shown that memory T cells can arise from cells that have previously transcribed IFN-γ or granzyme B genes (Harrington et al., 2008; Bannard et al., 2009). However, it is important to realize that these studies reveal little with regard to the developmental potential of individual naive T cells. Specifically, the fact that T cells that have a particular effector capacity can become memory T cells does not indicate that all naive T cells yield such effector cells, nor does it indicate that all memory T cells have gone through an effector phase.

To determine the developmental potential of naive T cells, it is essential to develop technologies in which T cell responses can be analyzed at the single naive T cell level. In early work that aimed to follow T cell responses at the clonal level, TCR repertoire analysis has been used to assess the kinship of T cell populations (Maryanski et al., 1996; Kedzierska et al., 2004). However, as several naive T cell clones can share the same TCR, it has been argued that such analyses do not necessarily monitor T cell fate at the single T cell level (Stemberger et al., 2007b; Obar et al., 2008). Recently, Stemberger et al. (2007a) have reported on a more elegant approach to address naive T cell potency. Using the transfer of single naive $CD8^+$ T cells into mice, this study provides direct evidence that a single naive $CD8^+$ T cell can form both effector and memory cell subsets. However, the statistical power of single-cell transfer studies obviously has limitations. In addition, if homeostatic proliferation would occur before antigen-driven proliferation in this system, this would limit the conclusions that can be drawn with regard to the pluripotency of a single naive T cell.

In this study, we have developed a technology that allows the generation of naive T cells that carry unique genetic tags (barcodes), and we describe how this technology can be used for the large-scale assessment of the developmental potential of single naive T cells. Using physiological frequencies of barcode-labeled naive $CD8^+$ T cells of different functional avidities, we demonstrate that in both systemic and local infection models, effector and memory $CD8^+$ T cell subsets share the same precursors in the naive T cell pool. These data demonstrate that under all conditions analyzed, single naive T cells do not selectively yield effector or memory T cells. Rather, T cell differentiation into effector and memory T cell subsets occurs by a one naive cell, multiple fates principle.

RESULTS

Generation of a barcode-labeled naive T cell pool

To study the lineage relationship between effector and memory $CD8^+$ T cells, we aimed to follow the progeny of individual naive $CD8^+$ T cells during the course of infection. Recently, we have developed a genetic tagging technology that allows lineage analysis in a high-throughput fashion (Schepers et al., 2008). In this technology, unique DNA barcodes are introduced into cell populations of interest. As these barcodes are transmitted to all progeny, microarray-based analysis of barcodes present in different cell populations can be used to reveal their common or separate ancestry.

A potential concern in using this technology for fate mapping within the T cell lineage is that the retroviral transduction procedure that is used to introduce barcode sequences requires T cell activation, which could influence subsequent T cell fate (note that lentiviral transduction strategies to modify quiescent mouse T cells have not been developed). To permit T cell fate mapping without a confounding effect of the barcoding procedure itself, we set out to develop a technology that allows the generation of "untouched" naive barcode-labeled T cells (Fig. 1 A). To this purpose, total thymocytes from young OT-I TCR-transgenic mice were transduced using a retroviral library containing ∼3,500 unique genetic tags plus a GFP marker gene (the barcode library). 1 d after transduction, ∼10%

Published May 17, 2010

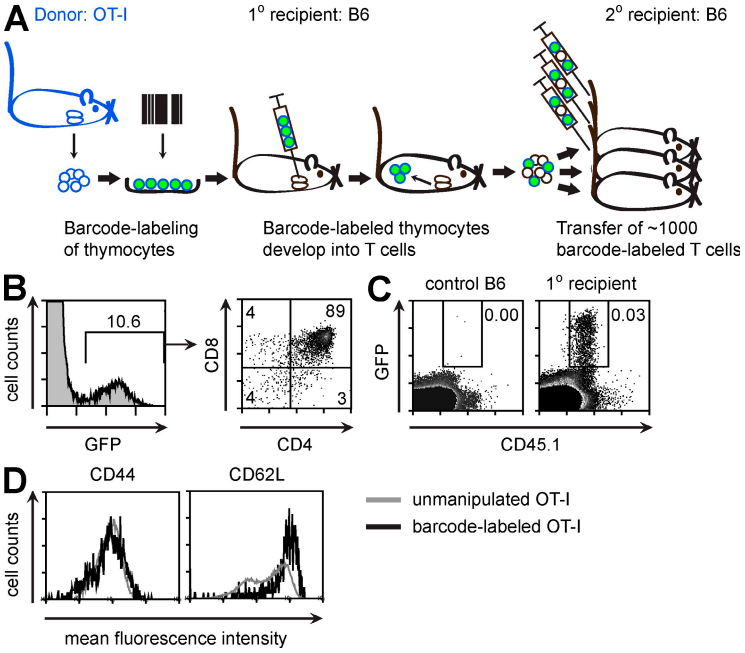

Figure 1. Genetic tagging of naive T cells. (A) Experimental setup for the generation and use of naive, barcode-labeled T cells. Donor thymocytes are transduced with a barcode library. Transduced cells are sorted and injected intrathymically into primary (1°) recipient mice. 3 wk later, mature T cells are isolated from 1° recipients, pooled, and transferred into 2° recipients. (B) Total CD45.1$^+$ OT-I thymocytes were transduced with the retroviral barcode library. 1 d after transduction, cells were stained and analyzed by flow cytometry. CD4 and CD8 expression is shown for the GFP$^+$ (barcode-labeled) population. Numbers indicate percentages. Data are representative of two independent experiments. (C and D) Sorted GFP$^+$ CD45.1$^+$ OT-I thymocytes were injected into the thymi of CD45.2$^+$ B6 1° recipient mice (n = 3). 3 wk later, spleen and lymph node cells were isolated, pooled, enriched for CD8$^+$ cells, stained for the indicated surface markers, and analyzed by flow cytometry. Data are representative of two independent experiments. (C) Expression of CD45.1 and GFP on gated CD8$^+$ cells from unmanipulated (control) B6 or 1° recipient mice. Numbers indicate percentages. (D) Expression of CD44 and CD62L on unmanipulated (CD45.1$^+$) and barcode-labeled (GFP$^+$ CD45.1$^+$) CD8$^+$ T cells.

of thymocytes showed GFP expression (Fig. 1 B), and the large majority (89%) of GFP$^+$ thymocytes was CD4$^+$CD8$^+$ (double positive; Fig. 1 B). Based on the kinetics of thymocyte maturation, it is likely that both proliferating double-negative and double-positive thymocytes contributed to the generation of these barcode-labeled cells (unpublished data; Egerton et al., 1990).

To investigate whether barcode-labeled thymocytes could be used to generate barcode-labeled naive T cells, GFP-expressing OT-I thymocytes were sorted and injected intrathymically into unmanipulated primary recipient mice. 3 wk after intrathymic injection, primary recipients contained a clear population of peripheral CD8$^+$ T cells that were GFP$^+$ (barcode labeled) and donor derived (CD45.1$^+$; Fig. 1 C). Importantly, these barcode-labeled CD8$^+$ T cells showed a naive phenotype, as indicated by the expression profiles of CD62L and CD44 (Fig. 1 D).

To test whether barcode-labeled OT-I cells behave similarly to unmanipulated OT-I cells upon activation, both were cotransferred into secondary recipients. Recipient mice were then infected with a *Listeria monocytogenes* strain expressing OVA (LM-OVA). Absolute peak heights of T cell responses cannot be compared because of the difficulty in determining the exact number of transferred barcode-labeled cells (see Materials and methods). However, the kinetics of expansion, contraction, and survival into the memory phase were comparable between barcode-labeled and unmanipulated OT-I cells (Fig. 2 A). Furthermore, both types of OT-I cells displayed a similar activated phenotype (CD44^{hi}, CD62L^{lo}, CD43^{hi}, CD127^{lo}, and mostly KLRG-1^{hi}; Fig. 2 B and Fig. S2).

Having established a strategy to generate naive barcode-labeled T cells, we investigated the potential of these cells for lineage tracking. Any effective lineage-tracking strategy must meet two criteria. First, it must be able to reveal a high degree of relatedness between two cell populations known to be derived from a common progenitor. Second, it must demonstrate the absence of relatedness when assessing two populations known to be derived from separate progenitors. To create an experimental setting in which related and unrelated cell populations coexist within a single mouse, secondary recipient mice received naive barcode-labeled OT-I cells and were challenged with both an $OVA_{(257–264)}$–expressing influenza strain (WSN-OVA) and $OVA_{(257–264)}$–expressing tumor cells (EL-4–OVA). In this setting, priming of naive T cells occurs independently and simultaneously in the lymph nodes that drain the two separate sites of antigenic challenge (Schepers et al., 2008). 5 d after infection, when activated T cells are still largely confined to the site of priming, lymph node cells were isolated and divided into two pools (samples A and B) per lymph node. These lymph node half-samples were independently expanded in vitro to boost T cell numbers before barcode analysis. As expected, the same barcodes were found in both half-samples of the same lymph node (Fig. 2 C, top left and middle plots). This indicates that cellular barcoding using naive barcode-labeled T cells is able to establish that these two T cell populations are progeny of the same naive T cell pool. In contrast, T cells isolated from two separate lymph nodes of the same mouse harbored a different set of barcodes (Fig. 2 C, top right plot), indicating that the technology can also correctly identify two T cell populations as being unrelated (i.e., derived from two different naive T cell pools). As a further control, barcode content was compared between T cell populations recovered from different mice. These "between-mice" comparisons are of use to reveal the background overlap that could, for instance,

Published May 17, 2010

arise in case of clonal dominance of a small number of thymocytes during reconstitution of primary recipients. Notably, the overlap in barcode content between such evidently unrelated samples was low (Fig. 2 C, bottom plot).

To quantify the degree of relatedness between different samples, the correlation between barcode signals was calculated (see Materials and methods). Analysis of lymph node samples from three mice revealed a consistently high positive correlation between barcode signals from two cell populations known to be related (samples A and B of the same lymph node; Fig. 2 D). In contrast, negative correlation values were obtained in all cases where two cell populations known to be unrelated were compared (Fig. 2 D). In conclusion, these data show that the introduction of genetic tags in thymocytes can be used to generate naive T cell populations suited for lineage tracking.

In all subsequent experiments, intrapopulation comparisons were included as a barcode sampling control to determine the reliability of barcode analysis for a given population, and between-mice comparisons were included to reveal the background overlap seen in a particular experiment. These two control comparisons of cells that are by definition related or unrelated set the boundaries for all biological analyses.

CD8+ T cells that are present during effector and resting memory phases are derived from the same naive T cells

Traditionally, memory T cells are defined on the basis of their long-term persistence after antigen clearance. More recently, it has been suggested that precursors of memory cells can already be identified around the peak of the response by the expression of high CD127 and low KLRG-1 levels (Kaech et al., 2003; Joshi et al., 2007). As a first test of the lineage

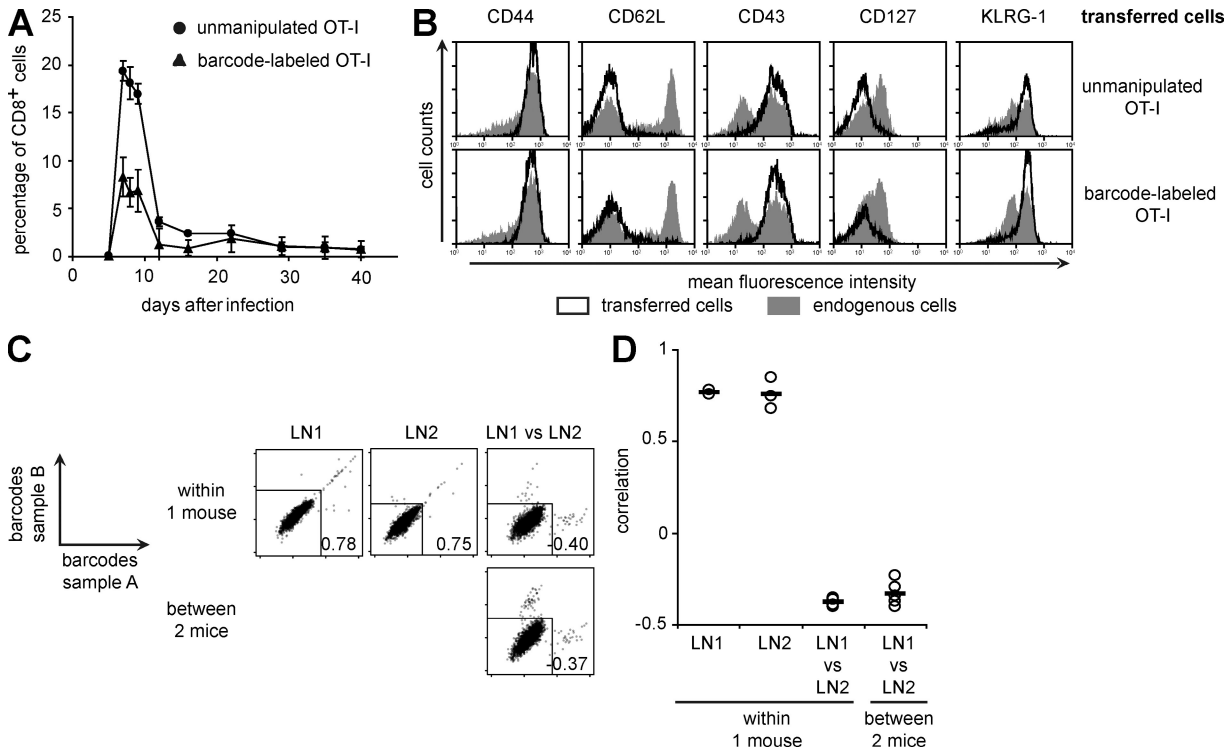

Figure 2. Barcode-labeled T cells can be used for lineage relationship analysis. (A) CD45.1+ B6 2° recipient mice (n = 5) received unmanipulated CD8+CD45.2+ OT-I cells plus naive barcode-labeled CD8+CD45.1+ OT-I cells and subsequent i.v. LM-OVA infection. Average responses of transferred OT-I cells are depicted; error bars indicate SD. (B) Naive, barcode-labeled or unmanipulated CD8+CD45.1+ OT-I cells were injected i.v. into CD45.2+ B6 2° recipient mice (n = 7 and 2, respectively). Mice were subsequently infected i.v. with LM-OVA. At day 7 after infection, blood cells were stained for the indicated surface markers and analyzed by flow cytometry. Shaded histograms represent total endogenous CD45.1−CD8+ T cells; black lines represent transferred CD45.1+ OT-I cells. One representative mouse per group is shown. Data are representative of two independent experiments. (C and D) Naive, barcode-labeled CD8+CD45.1+ OT-I cells were injected into CD45.2+ B6 2° recipient mice. Mice were subsequently challenged with WSN-OVA (i.n.) and EL-4 OVA tumor cells (s.c.) the next day. At day 5 after infection, lung- and tumor-draining lymph node cells were isolated, and each lymph node sample was split into two half-samples (samples A and B). Each half-sample was cultured separately for 3–4 d in vitro in the presence of 10 µg/ml IL-7 and 20 U/ml IL-2. Barcode analysis was performed independently on samples A and B of both lymph nodes (LN1 and LN2). Barcodes with a p-value of <0.001 were considered to be present above background. Rectangular dividers indicate which barcodes are present above background. Note that rather than fixing the absolute position of dividers in terms of intensity, it is the statistical probability of barcode presence that is kept constant for all samples in a given experiment. Data are representative of two independent experiments. (C) Representative 2-D plots of barcode analyses. Numbers indicate the correlation between signals from samples A and B. (D) Correlation analysis of barcodes present in T cells from the same or from distinct lymph nodes. Data are shown for three mice from two independent experiments. Mice from which barcodes in one out of the two draining lymph nodes could not be sampled reliably were excluded from further analysis.

Published May 17, 2010

relationship of effector and memory T cells, we performed a preliminary experiment to examine whether CD127^{hi}KLRG-1^{lo} and CD127^{lo}KLRG-1^{hi} CD8^{+} T cells are derived from the same or distinct naive T cells.

To this end, naive barcode-labeled OT-I T cells were injected into secondary recipient mice that were subsequently infected with LM-OVA. 10 d after infection, CD127^{hi}KLRG-1^{lo} and CD127^{lo}KLRG-1^{hi} CD8^{+} T cells were sorted from spleen and lymph nodes and each subset was divided into two half-samples (samples A and B; Fig. S3 A). As pilot experiments had shown that barcode copy numbers were too low for representative recovery from CD127^{hi}KLRG-1^{lo} cells, both half-samples of this subset were expanded separately in vitro to boost cell numbers before barcode analysis.

For all mice analyzed, barcodes were recovered representatively from the CD127^{lo}KLRG-1^{hi} subset (Fig. S3 B, top left plot; and Fig. S3 C), as indicated by the high correlation between barcode signals from samples A and B. Barcode signals from CD127^{hi}KLRG-1^{lo} half-samples were also well correlated, although some barcodes were only recovered from one of the two half-samples (Fig. S3 B, top middle plot; and Fig. S3 C). Furthermore, all between-mice comparisons showed the expected inverse correlation (Fig. S3 B, bottom plots; and Fig. S3 C, triangles).

Importantly, comparison of barcodes detected within the CD127^{lo}KLRG-1^{hi} and the CD127^{hi}KLRG-1^{lo} subset showed a strong correlation of barcode signals (Fig. S3 B, top right plot; and Fig. S3 C), demonstrating a high relatedness of both subsets. A small fraction of barcodes was only detected in one of the two subsets. However, this fraction of outliers was similar to that detected within intra–CD127^{hi}KLRG-1^{lo} comparisons. In line with this, the correlation of CD127^{lo}KLRG-1^{hi} versus CD127^{hi}KLRG-1^{lo} barcode comparisons was similar to that of intra–CD127^{hi}KLRG-1^{lo} comparisons (Fig. S3 C). Note that when two related populations are compared, of which one is sampled suboptimally, the intersample correlation approximates the lowest of the two intrasample correlations (Fig. S4, A and B). To further test the potential significance of the observed difference between CD127^{hi}KLRG-1^{lo} and CD127^{lo}KLRG-1^{hi} subsets, data were reanalyzed after exclusion of outliers present within the intrasubset comparison, a strategy that can be used to facilitate the detection of small differences (Fig. S4, C and D). Also after this filtering, no clear population of either CD127^{lo}KLRG-1^{hi}– or CD127^{hi}KLRG-1^{lo}–specific barcodes was observed (Fig. S4 E). Collectively, these preliminary data indicate that CD127^{lo}KLRG-1^{hi} and CD127^{hi}KLRG-1^{lo} subsets by and large share the same set of progenitors.

To address the kinship of effector and memory phase CD8^{+} T cells in a direct manner, we analyzed the barcode content of antigen-specific T cells that are present within the same mouse at different time points after infection. To this purpose, secondary recipient mice were infected with LM-OVA and blood was drawn for barcode analysis at the peak of the effector response. Animals were then kept until the resting memory phase, when both blood and spleen samples were obtained for barcode analysis. Analysis of sampling controls indicated that barcodes could be identified reliably during the memory phase and also in a small sample of peripheral blood obtained during the effector phase (Fig. 3 A, top plots).

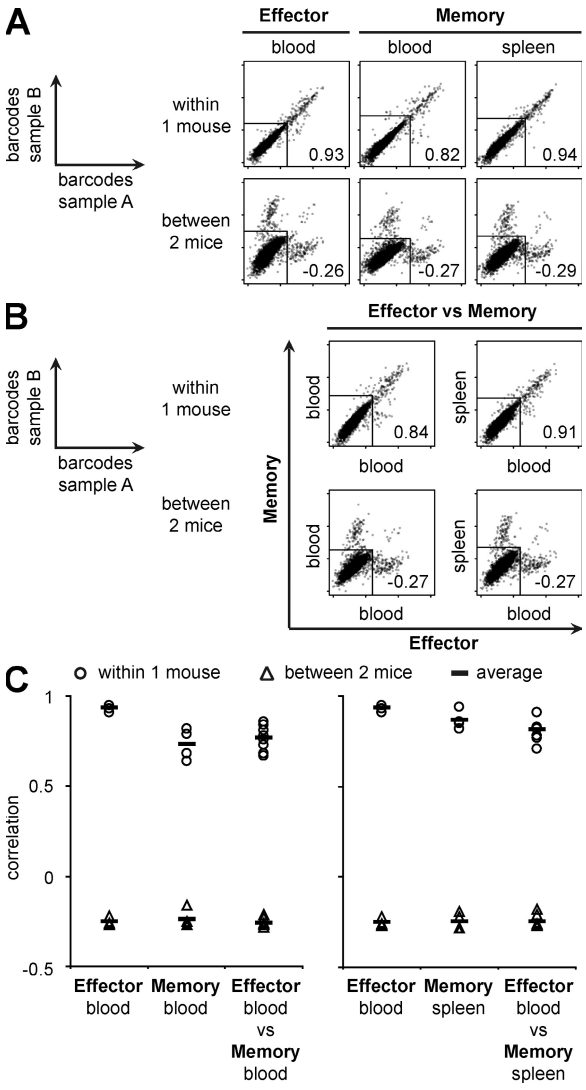

Figure 3. CD8^{+} T cells that are present during effector and resting memory phases are derived from the same naive T cells. CD45.2^{+} B6 2° recipient mice (n = 4) were injected with naive, barcode-labeled CD8^{+}CD45.1^{+} OT-I cells and subsequently infected i.v. with LM-OVA. Barcode analysis was performed on a 250–300-µl blood sample drawn at day 8 after infection (effector phase), and on a blood sample as well as on a spleen sample isolated at day 28 after infection (memory phase) from the same mice. Blood and spleen samples were divided into two halves (samples A and B) that were independently analyzed for barcode content. Barcodes with a p-value <0.005 were considered to be present above background. On average, 150 barcodes were detected per mouse. Data are representative of two independent experiments. (A and B) Representative 2-D plots of barcode comparisons. Numbers indicate the correlation between signals from samples A and B. (C) Correlation analysis of barcodes present in samples A and B from effector phase blood and memory phase blood (left plot) or effector phase blood and memory phase spleen (right plot). Data from four mice are depicted.

Published May 17, 2010

Between-mice comparisons demonstrated that these unrelated cell populations were also correctly identified as such (Fig. 3, A and B, bottom plots; and Fig. 3 C, triangles).

Importantly, when the barcode repertoire present in effector and memory phase samples was compared, it was apparent that the two were highly correlated, independent of whether the memory sample was drawn from blood (Fig. 3 B, top left plot; and Fig. 3 C) or spleen (Fig. 3 B, top right plot; and Fig. 3 C). Furthermore, few if any barcodes were identified that were selectively present in either the effector phase or the memory phase T cell population. These data demonstrate that $CD8^+$ T cells participating in the effector response and those present during memory phase in blood and spleen are derived from the same naive $CD8^+$ T cells.

$CD8^+$ T cells that are present in different lymphoid organs are derived from the same naive T cells

Previous work has suggested that the bone marrow can serve as a site of T cell priming (Feuerer et al., 2003). In addition, there is evidence to suggest that the bone marrow may contain a specialized memory T cell compartment (Palendira et al., 2008). Based on these data, it could be postulated that although effector and memory phase T cells in blood and spleen are derived from the same naive T cells, bone marrow–resident T cells may form a separate pool.

To investigate the lineage relationship of $CD8^+$ T cells that are found in different organs during the effector and memory phases, naive barcode-labeled OT-I T cells were transferred into secondary recipient mice. Mice were then infected with LM-OVA and barcode analysis was performed on cells isolated from blood, spleen, bone marrow, and lymph nodes at the peak of the effector response or during the memory phase. Barcodes were recovered efficiently from all four organs during the effector phase, albeit with a somewhat lower efficiency for lymph nodes and bone marrow (Fig. 4 A; and Fig. 4 B, circles), consistent with the lower number of barcode-labeled T cells isolated from these organs.

To assess whether T cells present at these distinct sites share common progenitors within the naive T cell pool, barcode content of the different T cell populations was compared. In all these comparisons, barcode content of T cells from the different anatomical sites was highly correlated and similar to the poorest sampled intraorgan comparison (Fig. 4 A; and Fig. 4 B, circles). This demonstrates that the progeny of naive T cells activated within an antigen-specific T cell response seeds all secondary lymphoid organs, including the bone marrow. Note that this analysis also validates the use of blood samples for lineage analysis during the effector phase (Fig. 3), as barcodes found in a 300-µl blood sample are representative of barcodes found in all other lymphoid organs at the peak of the effector response.

Barcode analysis was subsequently performed on cells isolated from blood, spleen, lymph node, and bone marrow samples at a late time point after infection (day 28; Fig. S5, A and B). Efficiency of barcode recovery was again high for spleen and blood, but lower for bone marrow and lymph nodes, consistent with the lower number of GFP^+ cells in these organs. Nevertheless, in all possible comparisons the interorgan correlation was similar to the correlation of the least efficiently sampled intraorgan comparison. Collectively, these data indicate that $CD8^+$ T cells that are present in different lymphoid organs are largely if not fully derived from the same set of antigen-specific precursors within the naive T cell repertoire.

Shared T cell families in resting memory and secondary T cell responses

To investigate whether all naive T cell clones of which the progeny persisted into resting memory phase also had descendants that were able to respond to secondary infection, naive barcode-labeled OT-I T cells were transferred into secondary recipients that were subsequently infected with LM-OVA. At the resting memory phase, cells from blood, spleen, lymph nodes, and bone marrow were isolated and pooled. Two parts were then used for independent barcode analysis and a third part was transferred into a tertiary recipient mouse that was thereafter infected with LM-OVA. At the peak of the secondary response, spleen samples were isolated for barcode analysis.

Analysis of the resting memory and secondary expansion sampling controls showed that barcodes could be reliably identified at both time points (Fig. 5 A, top left and middle plots; and Fig. 5 B). As expected, between-mice comparisons were poorly correlated, although higher than in previous experiments because of the larger number of participating barcodes in this experiment (Fig. 5 A, bottom plots; and Fig. 5 B, triangles).

Subsequent comparison of the barcode repertoire present in resting memory and secondary expansion samples showed that essentially the same barcode pool was present at both time points (Fig. 5 A, top right plot; and Fig. 5 B). Thus, these data show that all naive T cell clones that contribute to the resting memory population also have progeny that respond to secondary antigen encounter. This indicates that the kinship of effector and memory T cells applies not only to resting memory T cells but also to memory T cells as defined by their ability to respond to secondary antigen encounter.

Kinship of effector and memory phase $CD8^+$ T cells upon local infection

To establish whether the observed kinship of effector and memory subsets is restricted to systemic infection models, we determined the lineage relationship of these subsets in a local influenza A infection model. As pilot experiments had shown that the number of barcode-labeled cells in a blood sample drawn at the peak of the influenza-specific T cell response was too low for reliable barcode sampling, barcodes were read from a spleen sample obtained by partial splenectomy at the peak of the effector response. Mice were then kept until the resting memory phase, when the remainder of the spleen was analyzed for barcode content.

Sampling control comparisons demonstrated that barcodes could be read reliably during both the effector and

Published May 17, 2010

memory phases (Fig. 6 A, top left and middle plot; and Fig. 6 B). Between-mice controls showed the expected low correlation, although the number of shared barcodes was relatively high because of the higher amount of barcodes participating in this experiment (Fig. 6 A, bottom plots; and Fig. 6 B, triangles). Importantly, when barcode signals were compared between effector and memory phase samples, it was apparent that barcode content was highly correlated at both time points also during WSN-OVA infection (Fig. 6 A, top right plot; and Fig. 6 B). This demonstrates that effector and memory phase T cells are progeny of the same naive T cells also in a local infection model.

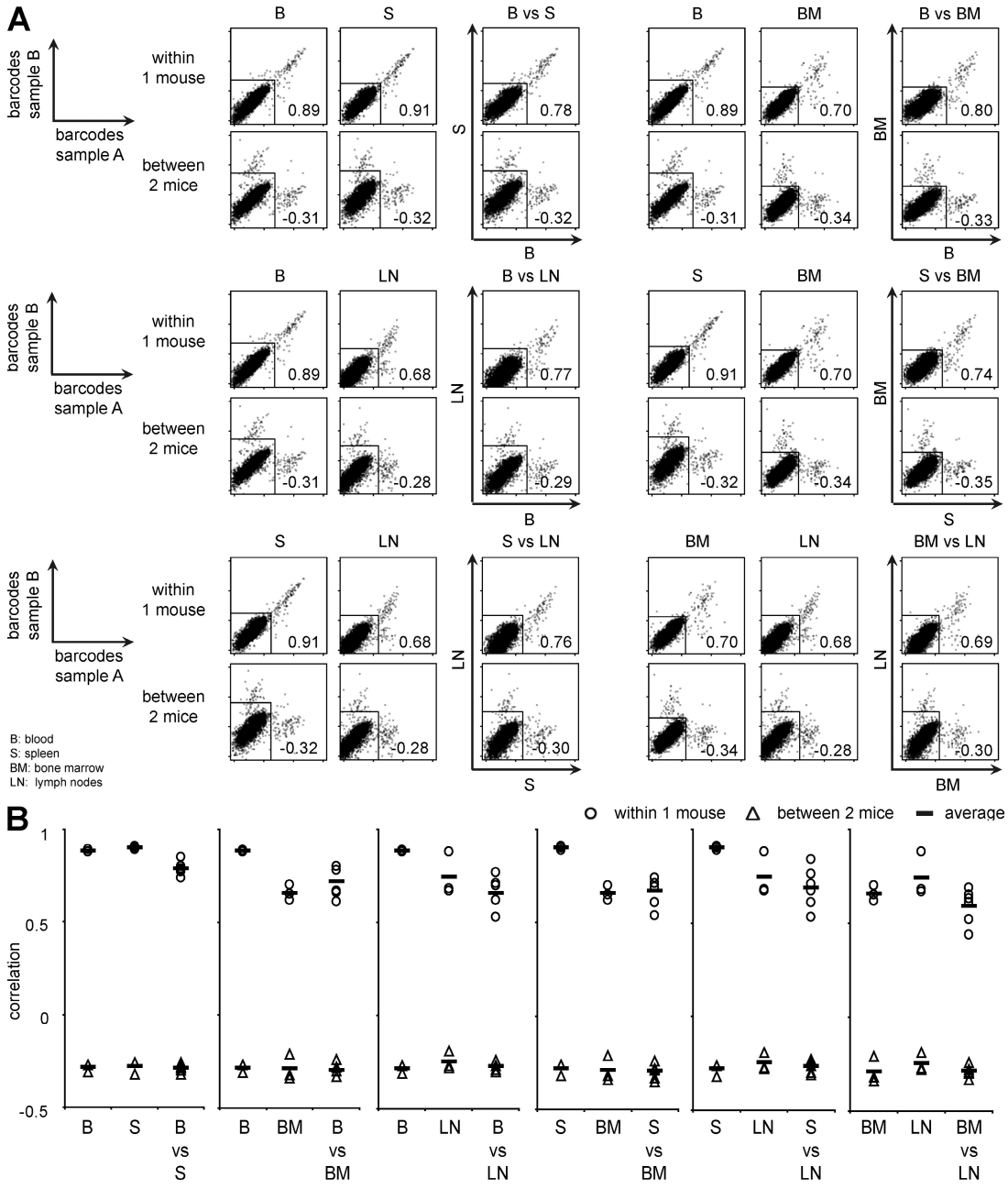

Figure 4. Effector phase CD8⁺ T cells present in blood, spleen, bone marrow, and lymph nodes are derived from the same naive T cells. CD45.2⁺ B6 2° recipient mice ($n = 3$) were injected with naive, barcode-labeled CD8⁺CD45.1⁺ OT-I cells and subsequently infected i.v. with LM-OVA. Barcode analysis was performed at day 8 after infection on cells recovered from blood, spleen, bone marrow, and lymph nodes. All samples were divided into two halves (samples A and B) that were independently analyzed for barcode content. Barcodes with a p-value <0.02 were considered to be present above background. On average, 150 barcodes were detected per mouse. S versus B comparisons are representative of two independent experiments; LN and BM barcodes were analyzed in one experiment. (A) Representative 2-D plots of barcode comparisons. Numbers indicate the correlation between signals from samples A and B. (B) Correlation analysis of barcodes present in samples A and B. Data from three mice are depicted.

Published May 17, 2010

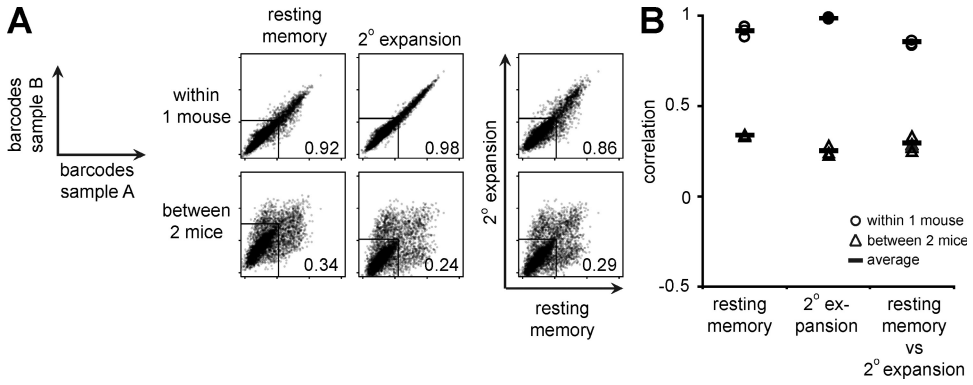

Figure 5. Naive T cell clones that contribute to the resting memory population also have progeny that respond to secondary antigen encounter. B6 2° recipient mice (n = 3) were injected with naive, barcode-labeled CD8$^+$ OT-I cells and subsequently infected i.v. with LM-OVA. 28 d after infection, blood, spleen, lymph node, and bone marrow cells were isolated, pooled per mouse, and divided into three parts. Two parts were used for barcode analysis (samples A and B, resting memory phase), and the third part was transferred into a B6 3° recipient mouse that was then infected with LM-OVA. 5 d later, barcodes were analyzed from spleen half-samples (2° expansion). Barcodes with a p-value <0.01 were considered to be present above background. On average, 1,080 barcodes were detected per mouse. (A and B) Representative 2-D plots of barcode comparisons. Numbers indicate the correlation between signals from samples A and B. (C) Correlation analysis of barcodes present in samples A and B. Data are derived from three 2° recipient and three 3° recipient mice analyzed within one experiment. These data confirm results obtained in an independent pilot experiment in which 1° expansion (effector phase) and 2° expansion memory populations could be compared for one mouse.

Relatedness of effector and memory T cells is independent of TCR avidity

As the naive T cell repertoire consists of a variety of clones that recognize the same antigen but with different avidities, we performed two experiments to address whether the lineage relationship of effector and memory subsets is dependent on the strength of the TCR–pMHC interaction.

To assess the lineage relationship of effector and memory CD8$^+$ T cells in an oligoclonal antigen-specific T cell population, we made use of Limited (Ltd) mice that express the OT-I TCRβ chain together with a Vα2 TCRα chain minilocus, which can recombine to form a limited repertoire of TCRs (Correia-Neves et al., 2001). This focused repertoire of TCRs expressed by Ltd T cells recognizes the OVA epitope with a range of avidities, as measured by K^b-OVA tetramer binding (van Heijst et al., 2009). Presumably because of the fact that only a single V segment is available for recombination, thymic selection of Ltd thymocytes is inefficient. Because of this low efficiency, it was technically not feasible to generate naive barcode-labeled Ltd cells by intrathymic injection of transduced thymocytes. Therefore, barcode labeling was performed on in vitro–activated peripheral Ltd T cells. After transfer into recipient mice and LM-OVA infection, the barcode content of effector and memory T cells was compared. Barcode sampling of the effector phase was less efficient in this preliminary experiment, possibly because of a

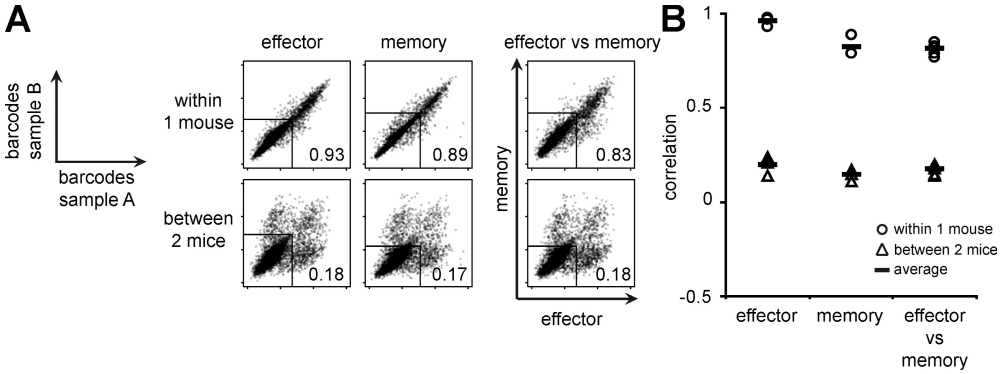

Figure 6. Kinship of effector and memory phase CD8$^+$ T cells upon local infection. B6 2° recipient mice (n = 4) were injected with naive, barcode-labeled CD8$^+$ OT-I cells and subsequently infected i.n. with WSN-OVA. Barcode analysis was performed on a one-fourth spleen sample obtained by partial splenectomy at day 9 after infection (effector phase), and on a spleen sample isolated at day 25 after infection (memory phase) from the same mice. Effector and memory phase samples were divided into two halves (samples A and B) that were independently analyzed for barcode content. Barcodes with a p-value <0.001 were considered to be present above background. On average, 800 barcodes were detected per mouse. (A and B) Representative 2-D plots of barcode comparisons. Numbers indicate the correlation between signals from samples A and B. (C) Correlation analysis of barcodes present in samples A and B. Data from four mice are depicted. These data confirm results obtained in an independent pilot experiment in which effector and memory phase populations could be compared for one mouse.

Published May 17, 2010

reduced clonal burst size of in vitro–activated T cells. Nevertheless, comparisons of effector and memory samples showed that barcodes in effector phase and secondary expansion phase T cells were largely shared (Fig. S6).

To study the kinship of effector and memory T cells in relation to T cell avidity in a system that does allow the use of naive barcode-labeled T cells, we made use of a recombinant *L. monocytogenes* strain (LM-Q4-OVA) that expresses a variant of the $OVA_{257–264}$ epitope. Functional recognition of this Q4 variant by OT-I T cells requires ∼18-fold more ligand than recognition of the parental epitope (Zehn et al., 2009). In line with the notion that Q4 forms a low avidity ligand, OT-I responses induced by LM-Q4-OVA have a reduced magnitude and earlier contraction (Zehn et al., 2009).

Barcode-labeled naive OT-I T cells were transferred into recipient mice that were challenged with LM-Q4-OVA at day 0 and rechallenged at day 27. At the peak of the effector response, barcodes were read from a spleen sample obtained by partial splenectomy and memory barcodes were read from the remainder of the spleen at the peak of the secondary response. Control comparisons showed that barcodes could be identified reliably during both the effector and the secondary expansion phases (Fig. 7 A, top left and middle plots; and Fig. 7 B), and that barcodes present in different mice were largely distinct (Fig. 7 A, bottom plots; and Fig. 7 B, triangles). In contrast, the barcode content of T cells present during effector and secondary expansion phases was highly correlated (Fig. 7 A, top right plot; and Fig. 7 B). This demonstrates that effector and memory cells are derived from the same naive T cells also for a lower avidity T cell response.

DISCUSSION

To date, our understanding of the process by which activation of naive T cells leads to formation of effector and memory T cells remains incomplete, with some studies favoring a principle of one naive cell, one fate and others favoring a principle of one naive cell, multiple fates (Reiner et al., 2007). The aim of this study was to determine which of these two principles applies to in vivo $CD8^+$ T cell differentiation.

Previous fate mapping studies were, with the exception of a study by Stemberger et al. (2007a), performed on the T cell population level, which precludes conclusions on the developmental potential of single naive T cells. To allow large-scale fate mapping of naive T cells at the single-cell level, we have developed a technology in which naturally cycling thymocytes are provided with unique genetic tags (barcodes) by retroviral transduction. Intrathymic injection of these genetically labeled thymocytes into unmanipulated recipient mice is then used to create a pool of naive barcode-labeled T cells. This strategy allows the use of genetic tagging for the analysis of T cell fate without any potential confounding effect of the in vitro T cell activation that is used for standard T cell gene modification. By following the progeny of physiological numbers of these naive barcode-labeled OT-I T cells during systemic or local infection, the lineage relationship of different T cell subsets could be assessed at the single-cell level.

The current large-scale analysis of naive $CD8^+$ T cell fate complements and extends the finding of Stemberger et al. (2007a), who used single-cell transfer to assess the formation of $CD8^+$ T cell subsets. Although the Stemberger study stands out as the first example of in vivo analysis of T cell fate at the single naive T cell level, several issues remained. First, in single-cell transfer studies it is difficult to exclude homeostatic proliferation as a confounding factor. Second, the possibility remained that selective differentiation into either effector or memory subsets would not occur during systemic T cell responses, in which inflammatory signals are omnipresent, but would take place upon local infection. Most importantly, the fact that a single naive T cell can form both effector and memory cells does not necessarily imply that all

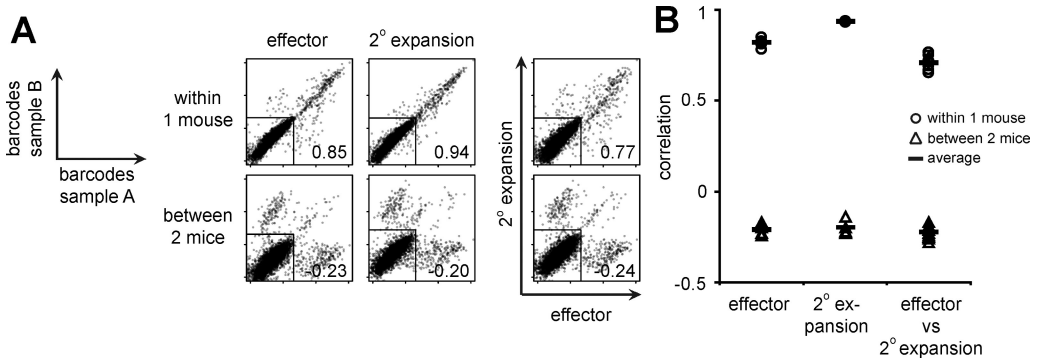

Figure 7. Relatedness of effector and memory T cells is independent of TCR avidity. B6 2° recipient mice ($n = 5$) were injected with naive, barcode-labeled $CD8^+$ OT-I cells and subsequently infected i.v. with LM-Q4-OVA. 27 d later, mice were rechallenged with LM-Q4-OVA. Barcode analysis was performed on a one-fourth spleen sample obtained by partial splenectomy at day 7 after infection (effector phase), and on a spleen sample isolated at day 5 after rechallenge (2° expansion) from the same mice. Effector and 2° expansion samples were divided into two halves (samples A and B) that were independently analyzed for barcode content. Barcodes with a p-value <0.005 were considered to be present above background. On average, 250 barcodes were detected per mouse. (A and B) Representative 2-D plots of barcode comparisons. Numbers indicate the correlation between signals from samples A and B. (C) Correlation analysis of barcodes present in samples A and B. Data from five mice analyzed within one experiment are depicted. Data were confirmed in a second experiment (five mice) performed with LM-A2-OVA, an *L. monocytogenes* strain containing another lower functional avidity variant of the OVA epitope (SAINFEKL).

Published May 17, 2010

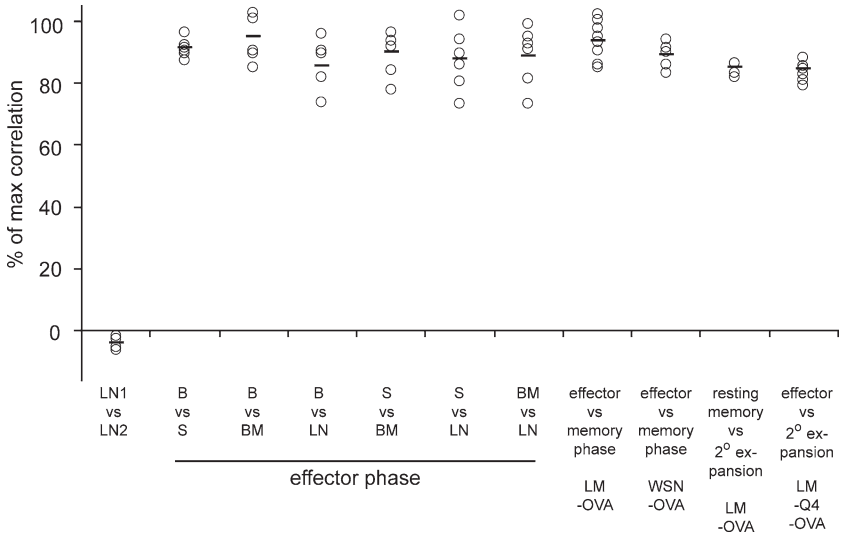

Figure 8. Relatedness of different T cell subsets. Results from barcoding experiments in Figs. 2, 3, 4, 5, 6, and 7 are depicted as the percentage of maximal attainable correlation. 100% reflects the mean correlation of all intrasample correlations for each individual experiment. 0% reflects the mean correlation of all between-mice comparisons for each individual experiment. Note that the average correlation of two sampling controls forms a reasonable estimate and possibly a slight overestimate of the maximal attainable correlation in case the two cell populations would be fully related (Fig. S4 B). From the effector versus memory phase comparison during LM-OVA infection, only the effector blood versus memory blood comparison is depicted. Circles represent correlations within individual mice; bars indicate group averages. B, blood; BM, bone marrow; LN, lymph nodes; S, spleen.

antigen-specific naive T cells, including T cells activated by a low avidity stimulus, follow this pathway of differentiation.

In this study, we provide strong evidence that effector and memory T cells present under different conditions of infection, and at different anatomical sites are in all cases derived from the same single naive T cells. Furthermore, this shared ancestry of effector and memory cells applies both to T cells that are activated by a low avidity and by a high avidity stimulus.

An important technical advance of the current approach for fate mapping is that it allows one to demonstrate that in case two unrelated T cell populations are present within an animal, such populations can readily be distinguished, something that is impossible in single-cell transfer systems. Specifically, the lack of kinship of T cells present in two different lymph nodes early after priming (Fig. 8, LN1 vs. LN2) forms a crucial control to remove any concerns on homeostatic proliferation of T cells before antigen-driven activation, something that would obviously limit the ability to visualize a difference in ancestry of different T cell subsets.

The difference in ancestry of T cell populations residing in different lymph nodes early after infection forms a very strong contrast to the shared ancestry of all other T cell populations examined (Fig. 8). Specifically, (a) effector and memory T cells are progeny of the same naive T cells, both when memory is defined by long-term persistence and when defined by capacity for secondary expansion; (b) effector and memory T cells are progeny of the same naive T cells, both in systemic and local infection models, and independent of the anatomical site in which they reside; and (c) effector and memory T cells are progeny of the same naive T cells in T cell responses of different functional avidities (Fig. 8).

These data argue against a model in which effector or memory fate is imprinted by distinct APC-derived signals delivered during initial priming. Likewise, a model assuming disparate fates for naive T cells that are primed early or late during infection is not supported by the data. Instead, the current data indicate that under a variety of conditions the dominant pathway of $CD8^+$ T cell differentiation is one naive cell, multiple fates.

MATERIALS AND METHODS

Mice. $CD45.1^+$ and $CD45.2^+$ C57BL/6 (B6) mice, as well as $CD45.1^+$ and $CD45.2^+$ TCR-transgenic OT-I and Ltd mice (provided by C. Nunes-Alves and M. Correia-Neves, University of Minho, Braga, Portugal) were bred and housed in the animal department of the Netherlands Cancer Institute (NKI). All animal experiments were approved by the Experimental Animal Committee of the NKI.

Retroviral transductions. Total thymocytes isolated from 4–8-wk-old $CD45.1^+$ OT-I donor mice were transduced by spin infection (90 min at 2,000 rpm) in the presence of 10 ng/ml of recombinant mouse IL-7 (PeproTech) and retroviral supernatant that had been incubated with 10 μg/ml DOTAP (Roche). Retroviral supernatants containing the barcode library (Schepers et al., 2008) were generated as previously described (Kessels et al., 2001) and diluted before use to reach a transduction efficiency of ~10%. 4 h after transduction, thymocytes were washed and cultured overnight in culture medium (IMDM/8% FCS/100 U/ml penicillin/100 μg/ml streptomycin/ 5×10^{-6} M 2-ME) supplemented with 10 ng/ml IL-7. Ltd cells were isolated from spleen and lymph nodes, activated for 2 d in culture medium containing 2 μg/ml concanavalin A (EMD) and 1 ng/ml IL-7, and subsequently transduced by spin infection in the presence of 10 ng/ml of recombinant mouse IL-7 and retroviral supernatant. Transduced Ltd cells were sorted on the basis of GFP expression and absence of staining with anti-B220 and anti-CD4 mAbs.

Intrathymic injection of transduced thymocytes. 1 d after transduction, thymocytes were purified using Lympholite (Cedarlane), and GFP^+ cells were sorted by FACS. Sorted cells were injected intrathymically into 4–6-wk-old primary (1°) recipient B6 mice. 1° recipients were sedated i.p. with azepromazine (1 μg/g body weight; Ceva Sante Animale) and anesthetized i.p. with a mixture of midazolam (7.5 μg/g body weight; Roche), fentanyl citrate (0.47 μg/g body weight; VetaPharma), and fluanisone (15 μg/g body weight; VetaPharma). For pain relief, carprofen (5 μg/g body weight; Pfizer) was given s.c. The fur overlying the thymus was disinfected with iodine and a small (1 cm maximum) longitudinal incision was made in the skin along the sternum. The salivary gland was pushed aside and each thymic lobe was injected with 25 μl of cell suspension. Thereafter, the skin was closed with two to three stitches. Each mouse received $0.5–1 \times 10^6$ sorted GFP^+ thymocytes.

Isolation, purification, and transfer of naive OT-I T cells. Barcode-labeled OT-I cells were isolated ~3 wk after intrathymic injections from spleen and lymph nodes (cervical, axillary, brachial, mesenteric, inguinal, and lumbar) of 1° recipient mice. $CD8^+$ cells were enriched by negative selection (Mouse CD8 T Lymphocyte Enrichment Set; BD). Enriched $CD8^+$ cells were pooled from several 1° recipients, and then analyzed by flow cytometry and/or transferred i.v. into several 8–10-wk-old B6 2° recipients (~1,000 barcode-labeled cells/2° recipient). This pooling and distribution approach guarantees that each 2° recipient receives an equal number of barcode-labeled T cells. In addition, it serves as an important control to ensure that the technology allows the detection of differences in kinship (between-mice controls). In all experiments, the number of transferred barcode-labeled cells, as indicated in the legends, is based on the analysis of very low percentages (~0.01%) of GFP^+ T cells and is therefore an approximation. On average, $\sim 2 \times 10^3$ barcode-labeled $CD8^+$ T cells were isolated per 1° recipient. Non–barcode-labeled OT-I cells were isolated from spleen and lymph nodes of OT-I mice.

***L. monocytogenes* and influenza A infections and tumor challenge.** 2° recipient mice were infected i.v. with 2.5×10^4 (1° infection) or 2.5×10^5 CFU (2° infection) of an *L. monocytogenes* strain expressing OVA (LM-OVA; provided by D. Busch, Institute for Medical Microbiology, Immunology, and Hygiene, Munich, Germany; Pope et al., 2001). Infection with LM-Q4-OVA, an *L. monocytogenes* strain expressing the SIIQFEKL sequence (Zehn et al., 2009), occurred at 2.5×10^3 (1° infection) or 2.5×10^5 CFU (2° infection) i.v. Alternatively, mice were anesthetized with ether and infected i.n. with 10^3 PFU of the recombinant influenza A/WSN/33 strain (WSN-OVA) that expresses the H-$2K^b$–restricted $OVA_{257–264}$ epitope (Topham et al., 2001), followed by s.c. injection of 10^7 EL4-OVA thymoma cells the next day (Kessels et al., 2001).

Recovery and in vitro expansion of transferred cells. Transferred OT-I or Ltd cells were recovered from spleen, bone marrow (femur, tibia, and iliac crest), lymph nodes (cervical, axillary, brachial, mesenteric, inguinal, and lumbar), and blood. Blood was drawn from the tail vein, cheek (~300 µl; in experiments in which mice were kept for longitudinal analysis), or heart (~800 µl; after sacrificing the mice). To recover barcode-labeled spleen cells from living mice, partial splenectomy was performed. Recovered cells were either used for flow cytometry or for barcode analysis. To allow for efficient barcode recovery, spleen, lymph node, and bone marrow samples were enriched for $V\alpha2^+$ cells by MACS (anti-PE MicroBeads; Miltenyi Biotec). Where indicated in the figures, cells were expanded in vitro for 3–4 d before Vα2 enrichment. All samples were divided into two equal parts (samples A and B) from which barcodes were recovered independently. This division was performed after Vα2 enrichment or, in case in vitro expansion was performed, before in vitro expansion.

Partial splenectomy. Mice were anesthetized with isoflurane and the skin overlying the spleen was shaved and disinfected. A <1-cm incision was made in the skin and peritoneum. One fourth of the spleen was resected and the wound on the spleen was closed with Histoacryl Topical Skin Adhesive (TissueSeal). Thereafter, the peritoneum and skin were closed with approximately three stitches and buprenorphine (0.1 µg/g body weight; Schering-Plough) was given as pain relief.

Flow cytometry. Cell-surface stainings were performed with the following reagents: Vα2-PE (B20.1), CD62L-PE (MEL-14), CD45.1-PE (A20), CD43-PE (1B11), streptavidin–PE-Cy7, CD4-allophycocyanin (APC; L3T4), CD8α–APC-Cy7 (53-6.7), KLRG-1–biotin (2F1), CD4-APC (RM4-5), B220-APC (RA3-6B2; BD), CD45.1-APC (A20; SouthernBiotech), CD127-PE (A7R34), CD44–Pe-Cy7 (IM7), CD127-APC (A7R34), and CD45.2-APC (104; eBioscience). Dead cells were excluded by DAPI staining. Analyses were performed on a $CyAn_{ADP}$ using Summit software (v4.3; both from Beckman Coulter). Cell sorting was performed on a FACSAria cell sorter using FACSDiva software (v5.0.1; both from BD) or a MoFlo high-speed sorter using Summit software (v3.1; both from Beckman Coulter).

Barcode recovery, microarray hybridizations and data analysis. Genomic DNA was isolated and barcode sequences were amplified by nested PCR as previously described (Schepers et al., 2008). PCR products were purified, labeled with cyanine-3 or cyanine-5, and cohybridized to the barcode microarray. Fluorescence signals were quantified and normalized, and duplicates were averaged. Barcodes present above background were defined for each sample based on the probability that a signal differed from a calculated background distribution (Schepers et al., 2008). The rectangular divider in two-dimensional (2-D) barcode plots indicates which barcodes are present above background based on the indicated probability (see figure legends). Note that rather than fixing the absolute position of dividers in terms of intensity, it is the statistical probability of barcode presence that is kept constant for all samples in a given experiment. The Pearson correlation between fluorescent signals of barcodes present within two samples was calculated. Calculations included a randomly drawn fraction of barcodes that were not present in a given sample (reference population), as described previously (Schepers et al., 2008). Note that the use of such a reference population within the calculations restricts correlation values to a range of 1 (full kinship) to approximately −0.5 (lack of kinship).

Online supplemental material. Fig. S1 depicts different models for the formation of effector and memory T cell subsets. Fig. S2 shows that activated barcode-labeled and unmanipulated OT-I T cells have a similar phenotype. Fig. S3 depicts the relatedness of $CD127^{lo}KLRG\text{-}1^{hi}$ and $CD127^{hi}KLRG\text{-}1^{lo}$ $CD8^+$ T cells. Fig. S4 shows how barcode analysis is interpreted when barcode sampling is suboptimal. Fig. S5 indicates that resting memory T cells present in different lymphoid organs are largely derived from the same naive T cells. Fig. S6 shows that effector and memory T cells in an oligoclonal antigen-specific T cell response are related. Online supplemental material is available at http://www.jem.org/cgi/content/full/jem.20091175/DC1.

We would like to thank A. Pfauth and F. van Diepen for cell sorting, W. Brugman for microarray production, D. Busch for providing LM-OVA, and C. Nunes-Alves and M. Correia-Neves for providing Ltd mice. We thank L. Rijswijk and T. Schrauwers for demonstrating the intrathymic injection and partial splenectomy, and S. Greven, M. Voetêl, and H. Grimminck for animal care and cheek bleedings. We also thank G. Bendle, A. Kaiser, and S. Naik for critically reading the manuscript.

M.J. Bevan was supported by grant U54 AI081680 from the National Institute of Allergy and Infectious Diseases.

The authors have no conflicting financial interests.

Submitted: 29 May 2009
Accepted: 16 April 2010

REFERENCES

Ahmed, R., and D. Gray. 1996. Immunological memory and protective immunity: understanding their relation. *Science*. 272:54–60. doi:10.1126/science.272.5258.54

Badovinac, V.P., B.B. Porter, and J.T. Harty. 2004. CD8+ T cell contraction is controlled by early inflammation. *Nat. Immunol.* 5:809–817. doi:10.1038/ni1098

Bannard, O., M. Kraman, and D.T. Fearon. 2009. Secondary replicative function of CD8+ T cells that had developed an effector phenotype. *Science*. 323:505–509. doi:10.1126/science.1166831

Chang, J.T., V.R. Palanivel, I. Kinjyo, F. Schambach, A.M. Intlekofer, A. Banerjee, S.A. Longworth, K.E. Vinup, P. Mrass, J. Oliaro, et al. 2007. Asymmetric T lymphocyte division in the initiation of adaptive immune responses. *Science*. 315:1687–1691. doi:10.1126/science.1139393

Correia-Neves, M., C. Waltzinger, D. Mathis, and C. Benoist. 2001. The shaping of the T cell repertoire. *Immunity*. 14:21–32. doi:10.1016/S1074-7613(01)00086-3

D'Souza, W.N., and S.M. Hedrick. 2006. Cutting edge: latecomer CD8 T cells are imprinted with a unique differentiation program. *J. Immunol.* 177:777–781.

Egerton, M., R. Scollay, and K. Shortman. 1990. Kinetics of mature T-cell development in the thymus. *Proc. Natl. Acad. Sci. USA*. 87:2579–2582. doi:10.1073/pnas.87.7.2579

Feuerer, M., P. Beckhove, N. Garbi, Y. Mahnke, A. Limmer, M. Hommel, G.J. Hämmerling, B. Kyewski, A. Hamann, V. Umansky, and V. Schirrmacher. 2003. Bone marrow as a priming site for T-cell responses to blood-borne antigen. *Nat. Med.* 9:1151–1157. doi:10.1038/nm914

Harrington, L.E., K.M. Janowski, J.R. Oliver, A.J. Zajac, and C.T. Weaver. 2008. Memory CD4 T cells emerge from effector T-cell progenitors. *Nature.* 452:356–360. doi:10.1038/nature06672

Jameson, S.C., and D. Masopust. 2009. Diversity in T cell memory: an embarrassment of riches. *Immunity.* 31:859–871. doi:10.1016/j.immuni.2009.11.007

Joshi, N.S., W. Cui, A. Chandele, H.K. Lee, D.R. Urso, J. Hagman, L. Gapin, and S.M. Kaech. 2007. Inflammation directs memory precursor and short-lived effector CD8(+) T cell fates via the graded expression of T-bet transcription factor. *Immunity.* 27:281–295. doi:10.1016/j.immuni.2007.07.010

Kaech, S.M., and R. Ahmed. 2001. Memory CD8+ T cell differentiation: initial antigen encounter triggers a developmental program in naïve cells. *Nat. Immunol.* 2:415–422.

Kaech, S.M., J.T. Tan, E.J. Wherry, B.T. Konieczny, C.D. Surh, and R. Ahmed. 2003. Selective expression of the interleukin 7 receptor identifies effector CD8 T cells that give rise to long-lived memory cells. *Nat. Immunol.* 4:1191–1198. doi:10.1038/ni1009

Kedzierska, K., S.J. Turner, and P.C. Doherty. 2004. Conserved T cell receptor usage in primary and recall responses to an immunodominant influenza virus nucleoprotein epitope. *Proc. Natl. Acad. Sci. USA.* 101:4942–4947. doi:10.1073/pnas.0401279101

Kessels, H.W., M.C. Wolkers, M.D. van den Boom, M.A. van der Valk, and T.N. Schumacher. 2001. Immunotherapy through TCR gene transfer. *Nat. Immunol.* 2:957–961. doi:10.1038/ni1001-957

Maryanski, J.L., C.V. Jongeneel, P. Bucher, J.L. Casanova, and P.R. Walker. 1996. Single-cell PCR analysis of TCR repertoires selected by antigen in vivo: a high magnitude CD8 response is comprised of very few clones. *Immunity.* 4:47–55. doi:10.1016/S1074-7613(00)80297-6

Masopust, D., S.M. Kaech, E.J. Wherry, and R. Ahmed. 2004. The role of programming in memory T-cell development. *Curr. Opin. Immunol.* 16:217–225. doi:10.1016/j.coi.2004.02.005

Obar, J.J., K.M. Khanna, and L. Lefrançois. 2008. Endogenous naive CD8+ T cell precursor frequency regulates primary and memory responses to infection. *Immunity.* 28:859–869. doi:10.1016/j.immuni.2008.04.010

Palendira, U., R. Chinn, W. Raza, K. Piper, G. Pratt, L. Machado, A. Bell, N. Khan, A.D. Hislop, R. Steyn, et al. 2008. Selective accumulation of virus-specific CD8+ T cells with unique homing phenotype within the human bone marrow. *Blood.* 112:3293–3302. doi:10.1182/blood-2008-02-138040

Pope, C., S.K. Kim, A. Marzo, D. Masopust, K. Williams, J. Jiang, H. Shen, and L. Lefrançois. 2001. Organ-specific regulation of the CD8 T cell response to *Listeria monocytogenes* infection. *J. Immunol.* 166:3402–3409.

Quigley, M., X. Huang, and Y. Yang. 2007. Extent of stimulation controls the formation of memory CD8 T cells. *J. Immunol.* 179:5768–5777.

Reiner, S.L., F. Sallusto, and A. Lanzavecchia. 2007. Division of labor with a workforce of one: challenges in specifying effector and memory T cell fate. *Science.* 317:622–625. doi:10.1126/science.1143775

Sarkar, S., V. Kalia, W.N. Haining, B.T. Konieczny, S. Subramaniam, and R. Ahmed. 2008. Functional and genomic profiling of effector CD8 T cell subsets with distinct memory fates. *J. Exp. Med.* 205:625–640. doi:10.1084/jem.20071641

Schepers, K., E. Swart, J.W. van Heijst, C. Gerlach, M. Castrucci, D. Sie, M. Heimerikx, A. Velds, R.M. Kerkhoven, R. Arens, and T.N. Schumacher. 2008. Dissecting T cell lineage relationships by cellular barcoding. *J. Exp. Med.* 205:2309–2318. doi:10.1084/jem.20072462

Stemberger, C., K.M. Huster, M. Koffler, F. Anderl, M. Schiemann, H. Wagner, and D.H. Busch. 2007a. A single naive CD8+ T cell precursor can develop into diverse effector and memory subsets. *Immunity.* 27:985–997. doi:10.1016/j.immuni.2007.10.012

Stemberger, C., M. Neuenhahn, V.R. Buchholz, and D.H. Busch. 2007b. Origin of CD8+ effector and memory T cell subsets. *Cell. Mol. Immunol.* 4:399–405.

Topham, D.J., M.R. Castrucci, F.S. Wingo, G.T. Belz, and P.C. Doherty. 2001. The role of antigen in the localization of naive, acutely activated, and memory CD8(+) T cells to the lung during influenza pneumonia. *J. Immunol.* 167:6983–6990.

van Faassen, H., M. Saldanha, D. Gilbertson, R. Dudani, L. Krishnan, and S. Sad. 2005. Reducing the stimulation of CD8+ T cells during infection with intracellular bacteria promotes differentiation primarily into a central (CD62LhighCD44high) subset. *J. Immunol.* 174:5341–5350.

van Heijst, J.W., C. Gerlach, E. Swart, D. Sie, C. Nunes-Alves, R.M. Kerkhoven, R. Arens, M. Correia-Neves, K. Schepers, and T.N. Schumacher. 2009. Recruitment of antigen-specific CD8+ T cells in response to infection is markedly efficient. *Science.* 325:1265–1269. doi:10.1126/science.1175455

van Stipdonk, M.J., G. Hardenberg, M.S. Bijker, E.E. Lemmens, N.M. Droin, D.R. Green, and S.P. Schoenberger. 2003. Dynamic programming of CD8+ T lymphocyte responses. *Nat. Immunol.* 4:361–365. doi:10.1038/ni912

Williams, M.A., and M.J. Bevan. 2007. Effector and memory CTL differentiation. *Annu. Rev. Immunol.* 25:171–192. doi:10.1146/annurev.immunol.25.022106.141548

Zehn, D., S.Y. Lee, and M.J. Bevan. 2009. Complete but curtailed T-cell response to very low-affinity antigen. *Nature.* 458:211–214. doi:10.1038/nature07657

SUPPLEMENTAL MATERIAL

Gerlach et al., http://www.jem.org/cgi/content/full/jem.20091175/DC1

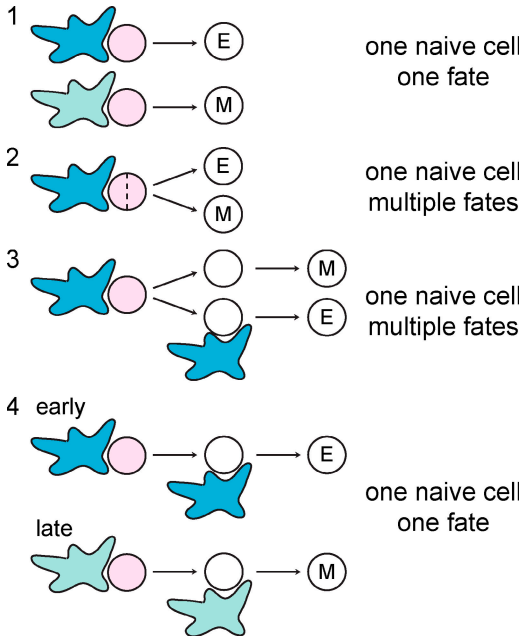

Figure S1. Models predicting effector and memory T cell lineage relationship. Schematic representation of four of the proposed models describing the lineage relationship of effector (E) and memory (M) T cells. Dendritic cells with different stimulating capacities are depicted in light and dark blue. Naive T cells are shown in pink. Note that other (variations on these) models have been proposed, but the fundamental distinguishing feature of the different models for the current study is whether they predict that single naive T cells produce single or multiple subsets.

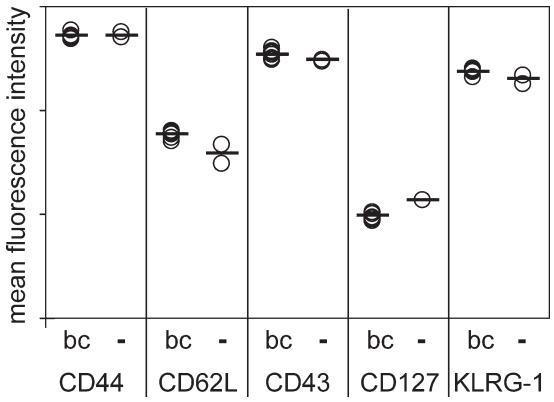

Figure S2. Phenotypic characterization of barcode-labeled and unlabeled OT-I T cells after LM-OVA infection. CD45.2$^+$ B6 2° recipient mice were injected with naive, barcode-labeled (bc) CD8$^+$CD45.1$^+$ OT-I cells or unmanipulated (−) CD8$^+$CD45.1$^+$ OT-I cells (n = 7 and 2, respectively). Mice were subsequently infected i.v. with LM-OVA. At day 7 after infection, blood cells were stained for the indicated surface markers and analyzed by flow cytometry. Circles represent individual mice; bars indicate group averages. Data are representative of two independent experiments.

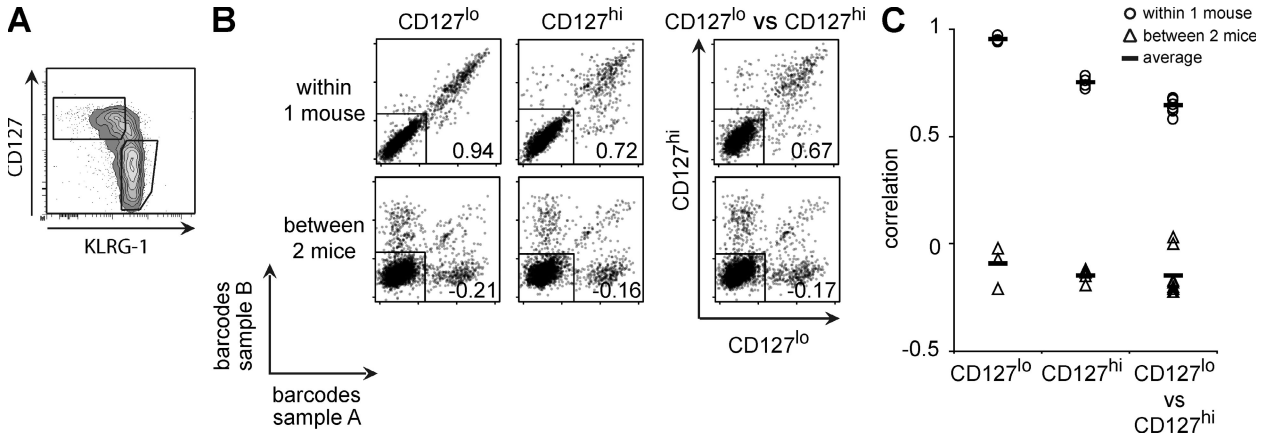

Figure S3. CD127^{lo}KLRG-1^{hi} and CD127^{hi}KLRG-1^{lo} cells are related. CD45.2^{+} B6 2° recipient mice (n = 4) were injected with naive, barcode-labeled CD8^{+}CD45.1^{+} OT-I cells and subsequently infected i.v. with LM-OVA. 10 d after infection, spleen and lymph node cells were isolated, enriched for CD8^{+} cells, and sorted into CD8^{+}, CD45.1^{+}, CD127^{lo}KLRG-1^{hi} and CD8^{+}, CD45.1^{+}, CD127^{hi}KLRG-1^{lo} cells. Data are derived from four mice analyzed within one experiment. (A) Flow cytometric sorting plot gated on CD8^{+}CD45.1^{+}GFP^{+} cells; sorting gates are indicated. (B and C) Both sorted populations, abbreviated as CD127^{lo} and CD127^{hi}, were divided into two halves (samples A and B) that were independently analyzed for barcode content. CD127^{hi} half-samples were separately expanded for 3 d in vitro in the presence of $OVA_{(257-264)}$–loaded splenic dendritic cells at a T cell/dendritic cell ratio of 10:1 before barcode analysis. Barcodes with a p-value <0.0001 were considered to be present above background. On average, 430 different barcodes were detected per mouse. (B) Representative 2-D plots of barcode comparisons. Numbers indicate the correlation between signals from samples A and B. (C) Correlation analysis of barcodes present in samples A and B. Data from four mice analyzed within one experiment are depicted.

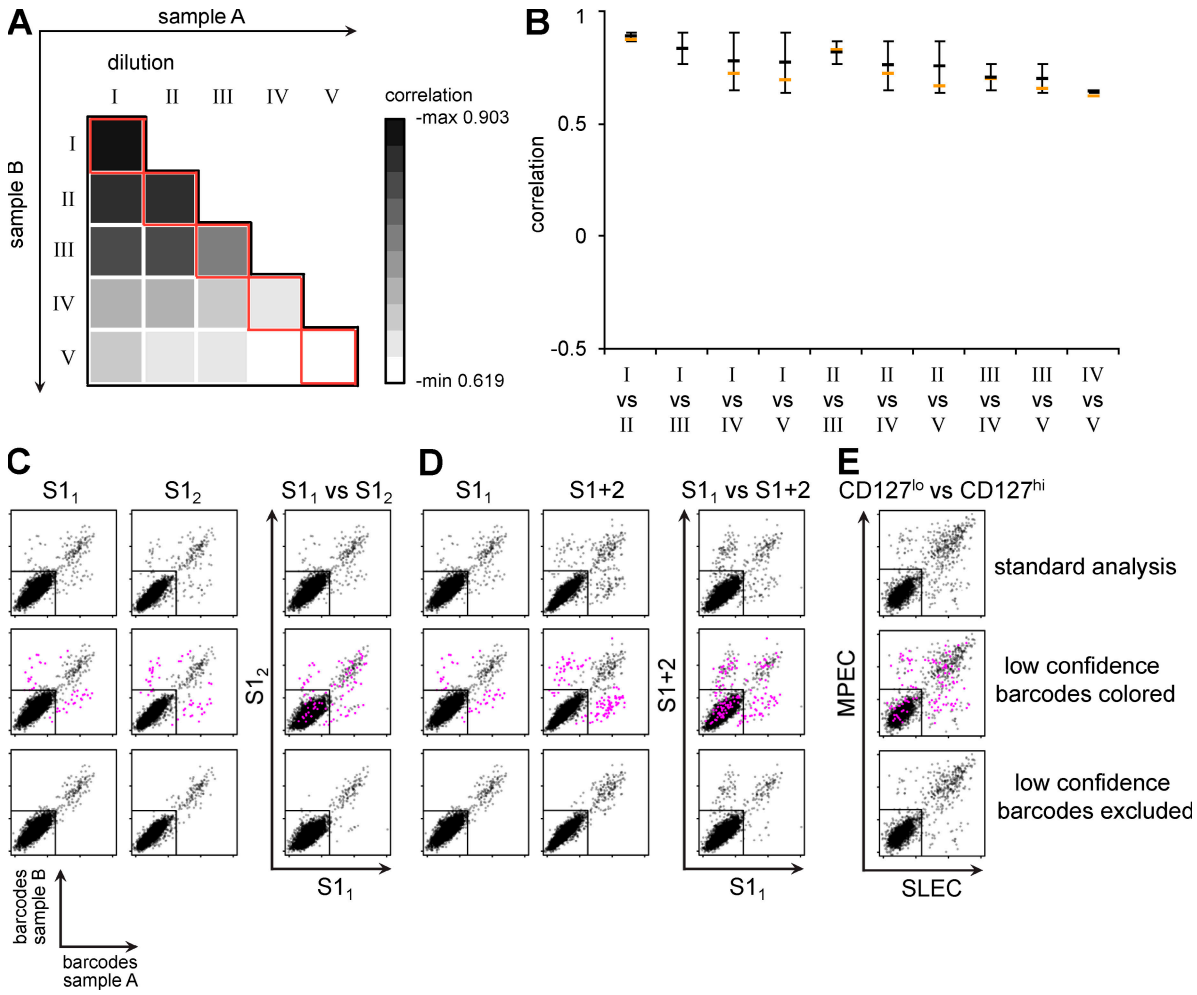

Figure S4. Barcode data analysis in a case of suboptimal sampling. CD45.2$^+$ B6 2° recipient mice were injected with naive, barcode-labeled CD8$^+$CD45.1$^+$ OT-I cells and subsequently received an i.v. infection with LM-OVA at days 0 and 30. 5 d later, genomic DNA was isolated from the spleen of two 2° recipient mice. (A and B) To determine how suboptimal sampling would affect correlation analyses on cell populations of which one is sampled less efficiently than the other, 1.5% of the spleen 1 DNA was diluted in four steps of twofold dilutions (dilutions I–V, with I being the highest and V being the lowest concentration). For each dilution, two samples were independently analyzed for barcode content. Barcodes with a p-value of <0.0001 were considered to be present above background. (A) The correlation of intradilution (red squares) and interdilution comparisons is depicted in a heat map. (B) The correlation of different interdilution comparisons (orange horizontal bars) is depicted in relation to the correlation of the two corresponding intradilution comparisons and their mean correlation (highest, lowest, and middle black horizontal bars, respectively). Note that when correlation analyses are performed for two samples that have substantially different intrasample correlation values (e.g., I vs. IV, I vs. V, and II vs. V), this value approximates that of the poorest intrasample comparison. (C and D) To test whether the exclusion of barcodes detected with low confidence would facilitate the detection of barcodes that are differentially present, part of the spleen 1 DNA was divided in two samples ($S1_1$ and $S1_2$) and part of the spleen 1 DNA was mixed with part of the spleen 2 DNA (S1+2). All three samples were diluted and split in two halves (samples A and B) for independent barcode analysis. Standard barcode analysis is shown in the first row. To statistically determine which barcodes are likely to be outliers (i.e., detected with low confidence), a linear model was fitted through the barcode signals from the intrasample comparisons and the studentized residuals were calculated per barcode. Barcodes with residuals ≥3 (97.5% chance of being an outlier) in the intrasample comparisons were either colored (second row) or excluded (third row). Barcodes with a p-value of <0.0005 were considered to be present above background. (C) Barcode comparison between two related samples ($S1_1$ vs. $S1_2$) in relation to the corresponding intrasample comparisons. (D) Barcode comparison between two partially unrelated samples ($S1_1$ vs. S1+2) in relation to the corresponding intrasample comparisons. (E) Barcode comparison between CD127^{lo}KLRG-1^{hi} (CD127^{lo}) and CD127^{hi}KLRG-1^{lo} (CD127^{hi}) cells from the experiment shown in Fig. S3. Standard barcode analysis is shown in the first row. Barcodes with residuals ≥3 in the intrasample comparisons were either colored (second row) or excluded (third row), as described for C and D. MPEC, memory precursor effector cell (CD127^{hi}KLRG-1^{lo}); SLEC, short-lived effector cell (CD127^{lo}KLRG-1^{hi}).

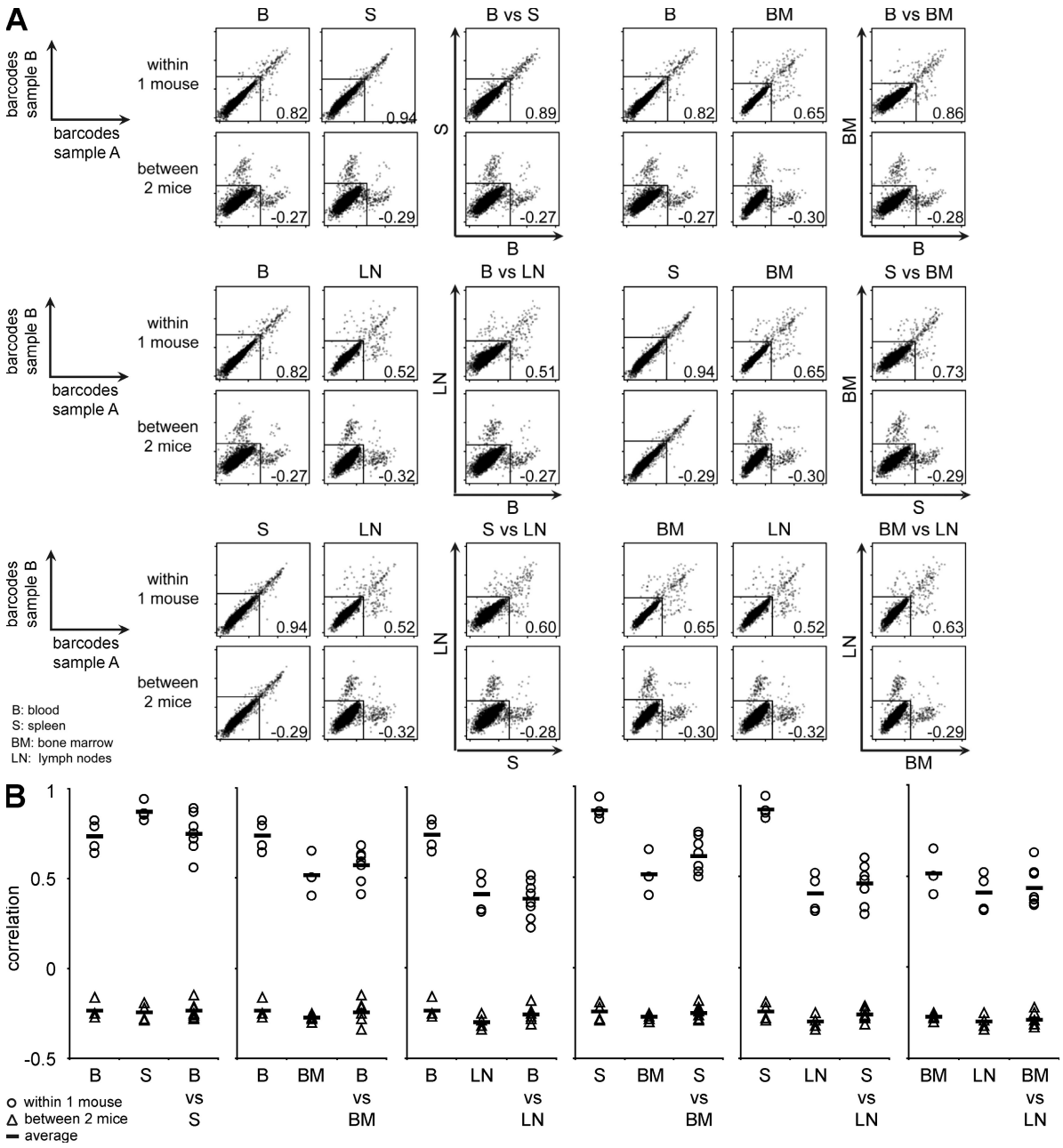

Figure S5. Memory CD8⁺ T cells present in different organs harbor the same set of barcodes. CD45.2⁺ B6 2° recipient mice ($n = 4$) were injected with naive, barcode-labeled CD8⁺CD45.1⁺ OT-I cells and subsequently received an i.v. infection with LM-OVA. Barcode analysis was performed on blood, spleen, bone marrow, and lymph node cells isolated at day 28 after infection. All samples were divided into two halves (samples A and B) that were independently analyzed for barcode content. Barcode comparisons are made between samples A and B taken from the same mouse (within one mouse) or from two different mice (between two mice). Barcodes with a p-value <0.005 were considered to be present above background. (A) Representative 2-D plots of barcode comparisons. Numbers indicate the correlation between signals from samples A and B. (B) Correlation analysis of barcodes present in samples A and B isolated from blood, spleen, bone marrow, and lymph nodes. Data from four mice analyzed within one experiment are depicted.

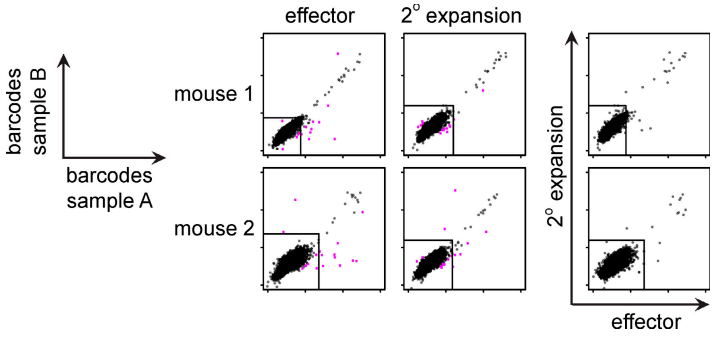

Figure S6. Relatedness of effector and memory T cells in an oligoclonal antigen-specific T cell response. B6 2° recipient mice were injected with barcode-labeled Ltd cells and subsequently infected i.v. with LM-OVA. 27 d later, mice were rechallenged with LM-OVA. Barcode analysis was performed on a 250–300-µl blood sample drawn at day 8 after infection (effector phase), and on a spleen sample isolated at day 5 after rechallenge (2° expansion) from the same mice. Blood and spleen samples were divided into two halves (samples A and B) that were independently analyzed for barcode content. Barcodes with a p-value $<10^{-8}$ were considered to be present above background. On average, 25 barcodes were detected per mouse. 2-D plots of barcode comparisons are shown for two mice within one experiment. All barcodes present in more than one mouse were excluded. To limit analysis to barcodes detected with high reliability, barcodes with residuals ≥3 (97.5% chance of being an outlier) in the intrasample comparisons (depicted in purple in the intrasample comparisons) were excluded in the intersample comparisons, as described for Fig. S3 (C and D). Note that this filtering procedure precludes the calculation of correlation values. Data from one experiment are depicted.